The Welding and Solidification Metallurgy of Alloy 625

Chemical composition and solidification microstructure are correlated to hot cracking susceptibility

BY M. J. CIESLAK

ABSTRACT. The weld metal microstructure development and solidification cracking behavior of Alloy 625 gas tungsten arc (GTA) welds as a function of composition has been determined. A three-factor, two-level, factorially-designed set of alloys involving the elements C, Si and Nb was examined. Differential thermal analysis (DTA) of these alloys indicated that Nb, and to a lesser extent C and Si, increased the melting/solidification temperature range. The DTA revealed that terminal solidification constituents were formed in the Nb-bearing alloys, the presence of which was confirmed by optical and electron microscopy techniques and identified as γ/MC-(NbC) carbide, γ/Laves and γ/M_6C carbide eutectic-type constituents. Addition of carbon to the Nb-bearing alloys was observed to promote the formation of the γ/MC(NbC) carbide constituent and Si was observed to promote increased formation of the γ/Laves constituent. Regression analysis of Varestraint hot-crack testing data revealed that additions of C or Si to Alloy 625 increased the susceptibility of the alloy to hot cracking. Niobium-free alloys were observed to have a very low tendency toward solidification hot cracking, but even among these alloys, C and Si additions were detrimental. It was concluded that the increased solidification temperature range and formation of Nb-rich eutectic constituents were primarily responsible for the increased susceptibility of Nb-bearing alloys to solidification cracking.

Introduction

Alloy 625 (58 minimum Ni-20–23 Cr, 8–10 Mo, 3.15–4.15 Nb+Ta-5 maximum Fe-0.5 maximum Mn, 0.5 maximum Si, 0.10 maximum C wt-%) has been a commonly used nickel-based alloy for over two decades. Although originally developed as a turbine alloy (Ref. 1), its combination of good oxidation and corrosion resistance and moderate mechanical strength have made it a successful alloy in many other applications. Among these are cladding and surfacing for marine environments (Refs. 2, 3) and for wear resistance as hardfacing for tool and die steels (Ref. 4).

Alloy 625 is not without its problems, though. Recent studies (Refs. 5, 6), have indicated that this alloy can be susceptible to hot cracking. Patterson and Milewski (Ref. 5) noted that hot cracked surfaces in arc welds made between Alloy 625 and 304L stainless steel were enriched in S, Nb, P and C, and that eutectic-like structures were present in the microstructures of these welds. Cieslak, *et al.* (Ref. 7), found that dissimilar metal CO_2 laser beam welds between Inconel Alloy 625 and 304 stainless steel made at slow travel speed (10 in./min) contained a Nb-rich Laves phase. Although in comparison to many other nickel alloys (Refs. 8, 9), Alloy 625 has a good reputation for resistance to hot cracking, it appears from the literature not to be totally immune from the problem.

A review of the literature reveals no published study that correlates the solidification microstructure with weldability in Alloy 625 as a function of chemical composition. In addition, no published report describes the sequences of solidification events leading to the development of the observed microstructure in Alloy 625. The purpose of this work, then, is twofold. First, the welding metallurgy of Alloy 625 is described in some detail. That is, the evolution of weld metal microstructure upon cooling from the liquidus is explained. Second, a correlation is established between alloy chemistry and both solidification microstructure and weldability (hot-cracking susceptibility). These results may provide for intelligent alloy optimization schemes for Alloy 625 and similar materials from a weldability perspective.

KEY WORDS

Microstructure Development
Solidification Crack
GTA Alloy 625 Welds
Differentional Analysis
Thermal Analysis
Eutectic Constituent
γ/Laves Constituents
γ/MC Carbide
γ/M_6 Carbide
Nb-Containing Alloys

Experimental Procedure

The alloy design decision for this experiment was driven by the desire to establish the fundamental solidification and hot-cracking mechanisms in this alloy system. The effect of tramp elements (S, P, B, etc.) on the solidification and weldability behavior of nickel-based alloys has been well established. It was concluded that studying these elements would not add much new insight. They were eliminated from this study by being held at constant low levels. Also, it had been observed earlier (Ref. 10) that the solidification microstructure in Alloy 625 and similar alloys could contain minor constituents composed of Laves phase and MC carbide. Both of these phases were Nb-rich and Laves had been shown (Ref. 11) to be stabilized by Si alloying additions. Based upon these two factors, C, Si and Nb were chosen as the composition variables for this experiment.

A three-factor, two-level factorial series of alloys was designed around these elements. The aim low level for C, 0.005 wt-%, was effectively the limit of industrial processing capabilities. The high level for C was set at what would likely be expected in a high C commercial heat of Alloy 625, 0.035 wt-%. The low level for Si was set as none intentionally added. The high level aim was 0.35 wt-%. The low level for Nb was set as none intentionally added. The high level aim was 3.5 wt-%. The levels for Nb would clearly indicate the difference between Nb-bearing and

M. J. CIESLAK is with Sandia National Laboratories, Albuquerque, N.Mex.

Paper presented at the 68th Annual AWS Meeting, held March 22–27, 1987, in Chicago, Ill.

Table 1—Alloy Compositions (wt-%)

Element	Alloy Number 1	2	3	4	5	6	7	8
C	0.006	0.031	0.006	0.036	0.009	0.038	0.008	0.035
Mn	0.02	0.02	0.02	0.03	0.03	0.03	0.03	0.03
P	0.005	0.005	0.005	0.005	0.006	0.006	0.006	0.006
S	0.002	0.002	0.002	0.003	0.003	0.003	0.004	0.003
Si	0.03	0.03	0.35	0.39	0.03	0.03	0.38	0.46
Cr	22.10	21.95	21.63	21.57	21.81	21.83	21.65	21.68
Mo	9.54	9.61	9.60	9.63	9.81	9.81	9.68	9.67
Ti	0.06	0.06	0.06	0.06	0.06	0.06	0.06	0.06
Nb	0.01	0.01	0.02	0.02	3.61	3.60	3.57	3.53
Fe	2.56	2.55	2.18	2.59	2.30	2.31	2.26	2.29
Ni	bal	bal	bal	bal	bal	bal	bal	bal

Nb-free alloys. The alloys were double vacuum melted at the Sandia National Laboratories melting and solidification facility. Initial melting was done in a vacuum induction furnace from virgin raw materials. Electrodes weighing approximately 150 lb (68.2 kg) were poured in vacuum. These electrodes were then vacuum arc remelted to 6-in. (152-mm) diameter ingots in preparation for hot working. Table 1 lists the compositions of the eight alloys studied.

Hot working of the ingots began with extrusion at 1175°C (2147°F) down to a 3-in. (76-mm) diameter bar. These bars were then flattened at 1175°C to approximately 0.6-in. plates. From these plates, specimens were taken for differential thermal analysis (DTA). The plates were further reduced by hot rolling (1175°C) to a thickness of approximately 0.18 in. (4.6 mm). Further reduction was done at room temperature to a thickness of approximately 0.12 in. (3 mm). These sheets were given a final anneal at 1010°C (1850°F) and water quenched. A cold straightening pass (<1% cold work) was then made to prepare the sheets for machining into Varestraint test specimens.

The autogenous gas tungsten arc (GTA) Varestraint test was used to quantify the susceptibility of these alloys to fusion zone hot cracking. The GTA welding parameters used were 100 A, (direct current, electrode negative at a travel speed of 8 in./min. The machine voltage was ≈ 12 V and argon was used as the shielding gas. These conditions produced welds that were approximately 0.20 in. wide at the top surface. The test specimens measured ≈ 6.5 × ≈ 1 × ≈ 0.12 in. (165 × 25 × 3 mm). All tests were performed at a strain level of ≈ 2.5% to simulate high restraint welding conditions. Replicate testing (4 to 5 tests per alloy) was employed to develop acceptable statistics. The order of testing was randomized to eliminate systematic error. Maximum crack length (MCL) was the quantitative measure of hot-cracking susceptibility used in this study.

Differential thermal analysis (DTA) testing was done on a Netsch thermal analyzer STA 429. Samples were machined from blocks taken from the hot-worked plates that had been subsequently annealed in vacuum at 1200°C (2192°F) for 4 h and water quenched. The samples weighed ≈ 0.8 g. All tests were conducted in a helium environment with pure W used as the reference material. To calibrate the system, pure Ni was found to melt within 2°C (3.6°F) of the established literature value. The experiments involved heating and cooling the Nb-bearing alloys (Alloys 5–8) through the melting/solidification temperature range as fast as was possible (20°C/min – 36°F/min) with the available equipment. The purpose of these experiments was to identify any terminal solidification reactions that were occurring in these alloys.

Varestraint test and DTA specimens were examined metallographically. After polishing through 0.05 μm alumina, they were electroetched (1–2 V) with 10% chromic acid for times necessary to reveal the structures of interest. Carbon-coated metallographic specimens were examined in the Hitachi 500 scanning electron microscope (SEM). Areas of interest were also analyzed with a Cameca MBX electron microprobe. In all cases, specimens were repolished flat and carbon coated prior to microprobe analysis. Point count analyses and profiles were carried out under the operating conditions of 15 kV and a beam current of ≈ 20 nA. K_α x-ray lines were used for analysis of all elements except Mo and Nb where L_α x-ray lines were used. The raw counting data were converted to weight percentages with a $\phi(\rho,Z)$ correction algorithm (Ref. 12).

High-resolution analyses of weld metal microstructures were performed using transmission electron microscopy (TEM) and analytical electron microscopy (AEM). Both thin foils and extraction replicas were examined. Specimens were examined in both a JEOL 200CX operating at 200 kV and a JEOL 100CX operating at 120 kV and equipped with a Tracor Northern EDS detector/spectrometer. Selected-area electron diffraction was used to identify the crystal structures of the various phases examined.

X-ray spectra collected in the AEM were reduced to weight percentages with the Cliff-Lorimer standardless-ratio technique (Ref. 13) with a data reduction program developed by Romig (Ref. 14). The Cliff-Lorimer k-factors were obtained experimentally for all elements analyzed except Si, where a suitable standard material was not available. In the case of Si, a calculated (Ref. 14) k-factor was used. K_α x-ray lines were used for the analysis of all elements. An absorption correction was not needed as the thin foil condition was never violated (Ref. 15). The AEM compositional data were obtained for the elements Ni, Fe, Cr, Nb, Mo and Si.

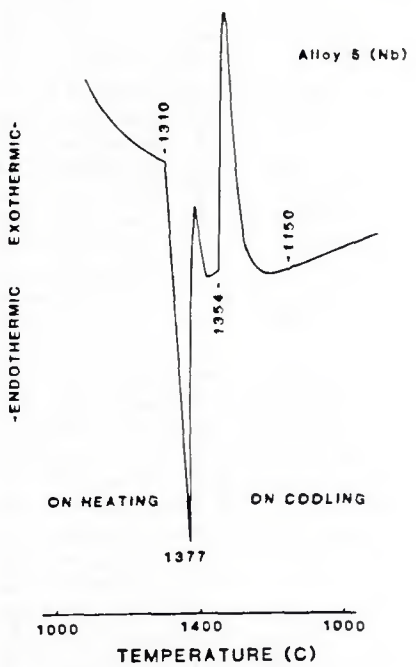

Fig. 1—DTA thermogram (20° C/min) for Alloy 5.

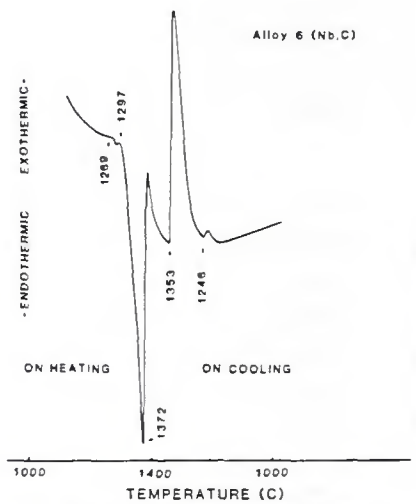

Fig. 2—DTA thermogram (20° C/min) for Alloy 6.

Results

The DTA thermograms obtained from Alloys 5–8 are shown in Figs. 1–4. The alloys containing C at the high level (6, 8) show an event prior to matrix melting, which is likely the dissolution of Nb carbide. The high-temperature annealing (4 h at 1200°C) was insufficient to dissolve these stable carbides. Figure 5 shows the Nb carbides present in the microstructure of Alloy 6 prior to DTA testing. The solidification behavior of Alloys 5–8 can be seen by examination of the individual thermograms. Alloys 5 and 6 show two exothermic events, while Alloys 7 and 8 show three exothermic events.

The results of Varestraint test experiments are shown in Fig. 6. As can be readily seen, the hot-cracking susceptibility under these test conditions is greater for the Nb-bearing alloys (5–8) than for the Nb-free alloys (1–4).

The microstructures observed in the GTA weld metals could be easily discriminated on the basis of Nb content. Alloys 1–4 had microstructures that were essentially single phase and will not be further discussed in this paper. Alloys 5–8 had microstructures that contained minor interdendritic constituents in addition to the dendritic matrix. As a general observation, Alloy 5 had the smallest minor constituent population and Alloy 8 had the greatest amount of minor constituent. No attempt was made to further quantify this observation in the weld metal. It had been shown earlier (Ref. 16) that the DTA samples had between 0.3% (Alloy 5) and 1.3% (Alloy 7) by volume of minor constituent. The SEM examination of Varestraint test samples from Alloys 5–8 revealed that these interdendritic constituents were associated with the formation of fusion zone hot cracks. As a representative example of these observations, Fig. 7 (A, B) shows the microstructure associated with a fusion zone hot crack in Alloy 7.

Identification of these phases was accomplished by performing selected-area electron diffraction on thin foils and extraction replicas made from the Varestraint test samples. The primary microconstituents observed were a Laves phase (hexagonal, a ≈ 0.476 nm, c ≈ 0.713 nm) and MC carbide (cubic, a ≈ 0.441 nm). The observations made in examination of the thin foils were consistent with the SEM examination of the Varestraint test samples relative to minor constituent population. That is, Alloy 5 had a much lower volume fraction of minor constituent than did Alloys 6–8. In addition to the Laves and MC carbide phases observed, Alloy 7 (high Nb, Si) was found to contain a coarsely lamellar M_6C carbide (diamond cubic, a ≈ 1.12 nm) constituent on its extraction replica. Two morphologies of MC were observed, a dendritic or "Chinese-script" morphology and a smaller blocky morphology.

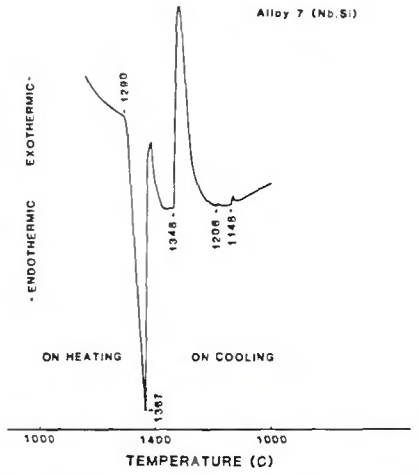

Fig. 3 – DTA thermogram (20° C/min) for Alloy 7.

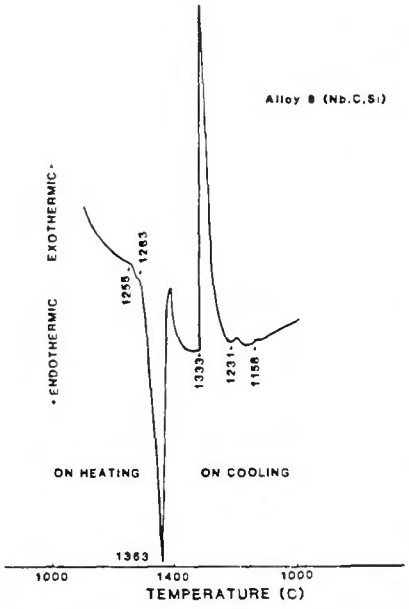

Fig. 4 – DTA thermogram (20° C/min) for Alloy 8.

It was qualitatively observed (Ref. 16) that the predominant microconstituent in Alloys 5 and 7 was Laves, whereas for Alloys 6 and 8, it was MC carbide. In the case of Alloy 8, large quantities of both MC carbide and Laves were observed. Figures 8A and 8B are representative TEM micrographs from Varestraint specimens showing MC carbide (Alloy 6) and Laves phase (Alloy 7), respectively. Table 2 summarizes the phases identified during the TEM analyses.

Two types of elemental segregation were observed in the GTA weld metals. The first was the discontinuous composition changes associated with the microconstituents observed. The second was the periodic pattern of dendritic segregation associated with the solidification process. Using AEM techniques, as described above, the compositions of the various phases in the weld metals of Alloys 5–8 were determined. These are listed in Table 3. In the cases of the carbide phases, a composition was calculated based upon ideal stoichiometry (MC or M_6C). As can be seen, all of the microconstituents are enriched in Nb and depleted in Ni relative to the nominal compositions.

The periodic dendritic segregation pattern representative of the GTA welds made on the Nb-bearing alloys is shown in Fig. 9 (Alloy 7). What is observed is the enrichment of Ni and Fe in dendrite core (DC) regions and the segregation of Nb, Mo and Si to interdendritic (ID) regions. There is very little dendritic segregation of Cr observed in this or any of the other alloys. Carbon could not be analyzed by this technique because of its low concentration. The interdendritic constituents associated with hot cracks in Alloys 5–8 were also chemically analyzed with the electron microprobe. The results of these analyses are given in Table 4. All constituents are enriched in both Nb and Mo relative to the nominal alloy compositions and the constituents observed in the high-Si heats (7 8) are enriched in Si.

Table 2—Phases Observed in the TEM

Alloy No.	Thin Foil	Extraction Replica
5 (Nb)	Laves[a]	Dendritic MC (NbC)[a]
	Small MC (NbC) carbides at γ/Laves interface	Blocky MC
		Laves
6 (Nb, C)	Dendritic MC (NbC)[a]	Dendritic MC (NbC)[a]
7 (Nb, Si)	Laves[a]	Impressions where Laves etched away[a]
	Small MC (NbC) carbides at γ/Laves interface	Small MC (NbC) carbides at prior γ/Laves interface
		Small dendritic MC (NbC)
		Coarsely lamellar M_6C
8 (Nb, C, Si)	Dendritic MC (NbC)[a]	Dendritic MC (NbC)[a]
	Laves in vicinity of MC (NbC)	Impressions where Laves etched away
	Small MC (NbC) carbides at γ/Laves interface	Small MC (NbC) carbides at prior γ/Laves interface

(a) Predominant structure observed.

Table 3—Phase Compositions (wt-%) from AEM Analysis

Alloy No.	Phase	Thin Foil/ Extraction	C	Ni	Fe	Cr	Nb	Mo	Si
5 (Nb)	Laves	T.F.		45.6 (0.2)[a]	1.4 (0.1)	15.6 (0.6)	19.2 (0.3)	18.2 (0.3)	<0.1
	Dendritic MC[b]	Extr.	12.1	3.3 (0.1)	0.3 (0.1)	4.1 (0.2)	73.4 (1.2)	7.2 (0.3)	0.0
	Blocky MC[b]	Extr.	11.6	0.1 (0.1)	0.0	1.3 (0.1)	82.6 (1.1)	4.4 (0.1)	0.0
6 (Nb, C)	Dendritic MC[b]	Extr.	11.9	2.1 (0.1)	0.1 (0.1)	4.1 (0.2)	65.5 (0.8)	16.3 (0.2)	0.0
7 (Nb, Si)	Laves	T.F.		48.2 (0.2)	1.0 (0.1)	13.9 (0.5)	18.2 (0.3)	17.6 (0.2)	1.2 (0.1)
	Dendritic MC[b]	Extr.	12.4	2.5 (0.1)	0.3 (0.1)	8.6 (0.4)	69.7 (1.1)	6.5 (0.2)	0.0
	Lamellar M_6C[c]	Extr.	2.8	31.6 (0.2)	0.5 (0.1)	14.6 (0.6)	31.0 (0.5)	18.7 (0.3)	0.9 (0.1)
	Blocky MC[b]	Extr.	12.3	3.5 (0.1)	0.0	7.4 (0.4)	68.5 (1.1)	8.2 (0.3)	0.0
8 (Nb, C, Si)	Laves	T.F.		46.7 (0.2)	0.9 (0.1)	13.6 (0.5)	16.8 (0.2)	19.8 (0.3)	2.2 (0.1)
	Dendritic MC[b]	Extr.	12.2	4.5 (0.1)	0.4 (0.1)	5.2 (0.2)	60.0 (0.8)	17.7 (0.3)	0.0
	Blocky MC[b]	Extr.	12.2	4.1 (0.1)	0.4 (0.1)	5.1 (0.3)	65.0 (1.2)	13.2 (0.4)	0.0

(a) Absolute error, wt-%.
(b) Calculated assuming ideal MC stoichiometry.
(c) Calculated assuming ideal M_6C stoichiometry.

Table 4—Compositions of Constituents Associated with Hot Cracks

Alloy No.	Nb	Si	Ni	Mo	Cr	Fe
5	17.45[a] (1.64)[b]	0.07 (0.04)	48.18 (1.98)	15.32 (2.11)	17.32 (0.46)	1.48 (0.10)
6	17.42 (1.63)	0.08 (0.03)	48.17 (2.00)	15.32 (2.07)	17.31 (0.49)	1.47 (0.10)
7	15.49 (0.61)	1.53 (0.10)	51.86 (0.75)	13.67 (0.53)	15.78 (0.32)	1.43 (0.04)
8	15.21 (0.64)	1.75 (0.33)	50.21 (1.10)	15.10 (1.03)	16.11 (0.64)	1.44 (0.12)

(a) All values in weight percent.
(b) Standard deviation from multiple measurements.

Discussion

Microstructural Evolution during Solidification

The development of microstructure in weldments is intimately related to the segregation of alloying elements during solidification. Terminal solidification constituents form when the solid solubility for particular elements in the growing cells or dendrites is exceeded. In cellular or dendritic growth these phenomena lead to the distribution of alloying elements in accordance with the thermodynamic (phase diagram) requirements of the system. An alloying element having distribution coefficient (k) less than unity will be depleted at the dendrite cores and enriched in interdendritic regions.

In the case of Alloy 625, C, Si and Nb have distribution coefficients less than unity (Ref. 16). The partitioning of these elements to interdendritic regions (Fig. 9) during solidification results in the formation of the terminal eutectic-like constituents as the solid solubility of the γ matrix dendrites is exceeded. The DTA thermograms show the events that occur during the melting and solidification of Alloys 5-8. The interpretation of these data have been reported recently by Cieslak, *et al.* (Ref. 16), and will only be summarized briefly here. The liquidus temperatures for Alloys 5-8 are (Ref. 16) 1377°, 1372°, 1367° and 1363°C (2511°, 2502°, 2493° and 2485°F), respectively. Indications representing the formation of the γ/Laves constituent in Alloys 5, 7 and 8 occur at 1150°, 1148° and 1158°C (2102°, 2098° and 2116°F), respectively. Indications representing the formation of the γ/MC (NbC) constituent in Alloys 6 and 8 occur at 1246°C (2275°F) and 1231°C (2248°F), respectively. The indication representing the formation of the γ/M_6C constituent in Alloy 7 occurs at 1206°C (2203°F).

The results of the electron microprobe analyses of alloying element segregation patterns both within dendrites and interdendritic constituents clearly indicate that the segregation of Nb is the controlling factor in the development of solidification microstructure in these alloys. The Nb concentration in these constituents (γ/MC (NbC), γ/Laves and γ/M_6C) is many times greater than the bulk alloy concentration. Silicon also partitions quite strongly to the interdendritic constituents in Alloys 7 and 8. Individual phases could not be discerned by these analyses.

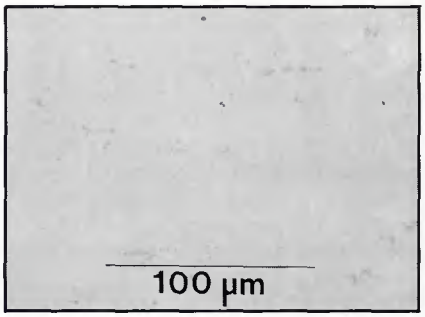

Fig. 5—Niobium carbides in Alloy 6 after 4 h at 1200°C and subsequent water quenching.

The results of the TEM analysis (Table 3) of the weld metals from Alloys 5-8 reveal the effects of C and Si alloying additions on Alloy 625 microstructure. In the absence of intentional C or Si additions (Alloy 5), Laves is the predominant structure observed during thin-foil analysis. The amount of this constituent, though, is quite small, consistent with the DTA thermogram (Fig. 1) signal for this event at a level just above background. When C is added (0.038 wt-%, Alloy 6) to Alloy 625, only MC (NbC) carbide is observed (at the expense of Laves) in both thin foils and extraction replicas. In this alloy, formation of the γ/Laves constituent is apparently precluded by alloying with this level of C. (The presence of a small amount of γ/Laves constituent in this alloy, not detectable by either DTA or TEM techniques, cannot be unequivocally discounted.) When Si is added (0.38 wt-%, Alloy 7) to Alloy 625, Laves is again the predominant phase observed in the microstructure, but now in an amount far greater than that observed in Alloy 5. In addition, M_6C carbide is also observed. Table 3 shows that the M_6C carbide is enriched in Nb, Mo and Si. It has been shown previously that Si promotes the formation of Mo-rich M_6C carbides both as a γ/M_6C eutectic-type constituent (Ref. 17) and in the solid state (Ref. 18) in austenitic Fe and Ni alloys. Laves phase is also enriched in Si. It is interesting to note that while Laves phase is structurally of the type A_2B, no Ni_2Nb phase has been found to exist. A ternary Laves phase of the form Ni_3SiNb_2 has been observed by Bardos, *et al.* (Ref. 19), clearly indicating the stabilizing influence of Si on Laves. When both C and Si are added to Alloy 625 (0.035 wt-% C, 0.46 wt-% Si, Alloy 8), both MC (NbC) carbide and Laves are observed in both thin foils and extrac-

tions consistent with the two minor peaks on the DTA thermogram—Fig. 4. Again, the Laves is found to be enriched in Si—Table 3. With Si present in the alloy, the γ/Laves constituent is not precluded from forming even though C is also intentionally alloyed. A more detailed description of the evolution of the solidification microstructure in these alloys has been given recently by Cieslak, *et al.* (Ref. 16).

The microstructural modification in these alloys as a function of the minor elements C and Si is remarkable but not without precedence. Nakao, *et al.* (Ref. 20), studied the effects on microstructure caused by alloying IN-519 (Fe-24Cr-24Ni-3Nb wt-%) with C and Si. At low C levels (0.02-0.03 wt-%), γ/Laves was the only solidification constituent observed in weld metal. As C content was increased (>0.2 wt-%) the γ/Laves constituent was replaced by γ/MC (NbC) constituent in a manner analogous to that observed in the present study. The γ/MC constituent solidified at a higher temperature than the γ/Laves constituent, also consistent with the results of the present work on Alloy 625.

In summary, the evolution of solidification microstructure in Alloy 625 fusion welds is dominated by the segregation of Nb. The particular interdendritic constituents observed (e.g., γ/Laves and γ/MC) in a given heat of Alloy 625 are influenced by the concentration of the elements C and Si. These constituents are not observed when Nb is not present.

Weldability Analysis

In the early development of analysis of Varestraint test data, Savage and Lundin (Ref. 21) interpreted maximum crack length as a measure of the hot-cracking temperature range. More recently, a similar approach has been adopted by Matsuda and coworkers (Ref. 22) in their interpretation of trans-Varestraint test data. Their brittleness temperature range (BTR) parameter is obtained from the maximum crack length achieved at high levels of applied strain during trans-Varestraint testing. From a metallurgical viewpoint, they suggested that the BTR could be correlated to the existence of a two-phase, liquid-plus-solid structure in an alloy. The lower limit of the BTR could extend down to the terminal solidification reaction of a nonequilibrium eutectic-type constituent.

The general correlation between weldability and solidification behavior can be traced back to early investigators (Refs. 23, 24) who concluded that alloys having wider solidification temperature ranges would be more crack susceptible than alloys having narrow solidification temperature ranges. The first to quantify this understanding was Borland (Ref. 24), who attempted to determine the hot-cracking

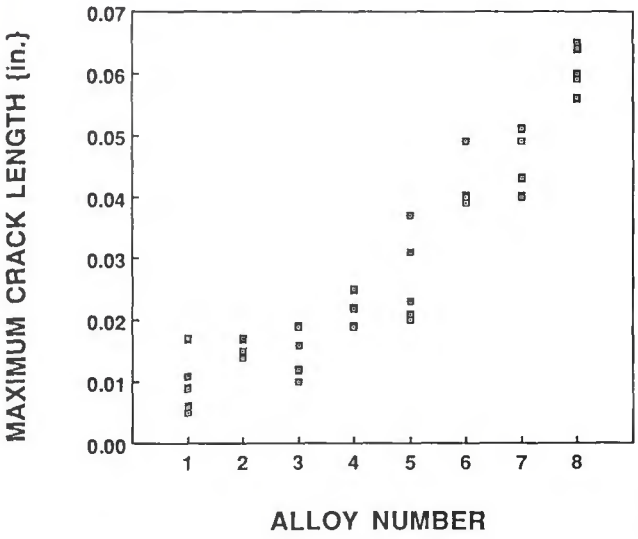

Fig. 6—Varestraint test results for Alloys 1-8.

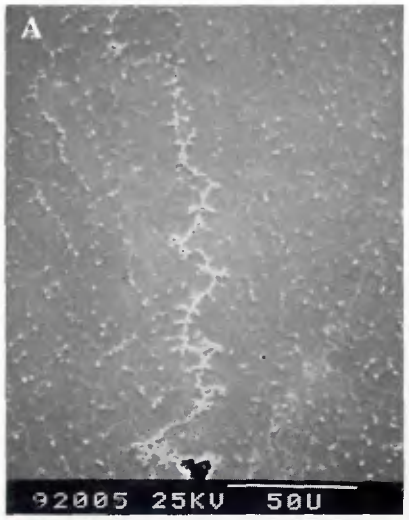

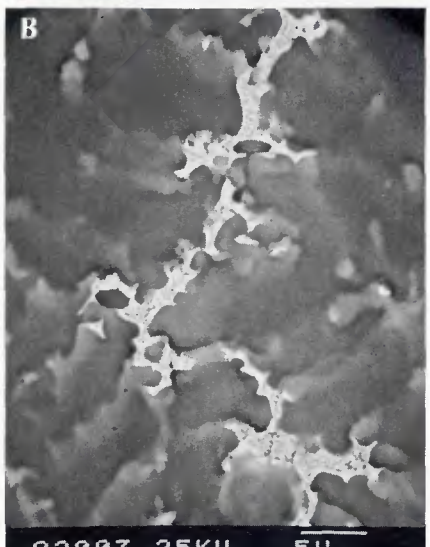

Fig. 7—A—SEM image of microstructure associated with hot cracks in Alloy 7; B—higher magnification SEM image showing constituent morphology in greater detail.

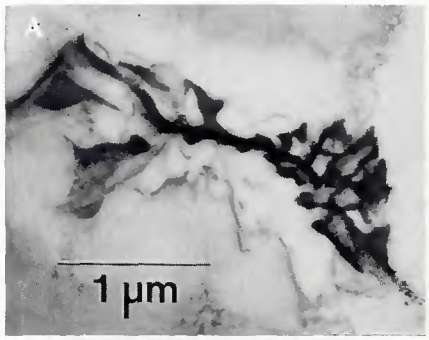

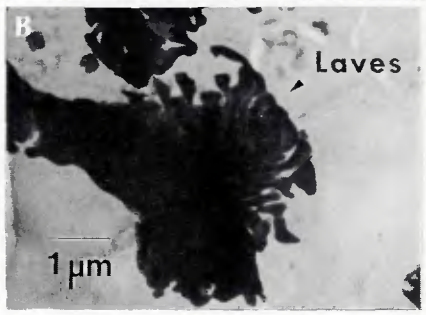

Fig. 8— A—TEM micrograph of MC carbide morphology in Alloy 6 Varestraint test specimen; B—TEM micrograph of Laves morphology in Alloy 7 Varestraint test specimen.

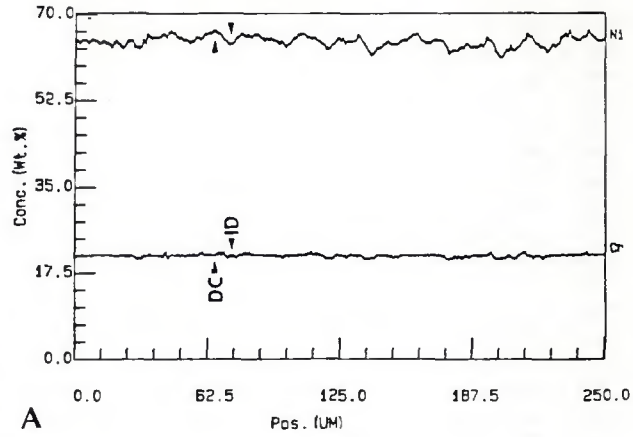

Fig. 9—Microprobe profile showing dendritic segregation pattern in Alloy 7. A—Ni, Cr; B—Mo, Nb; C—Fe, Si. DC indicates a dendrite core position, and ID an interdendritic position.

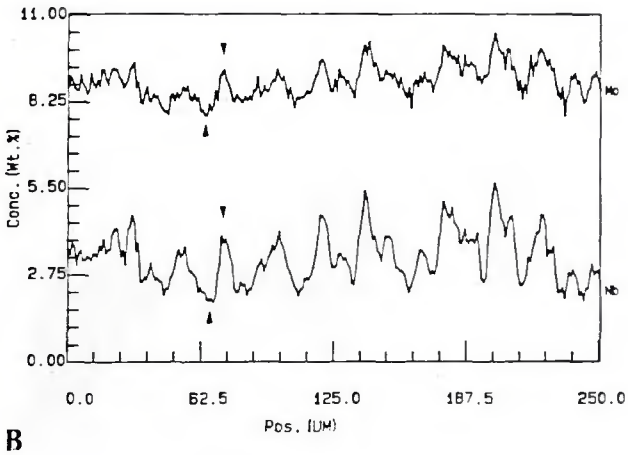

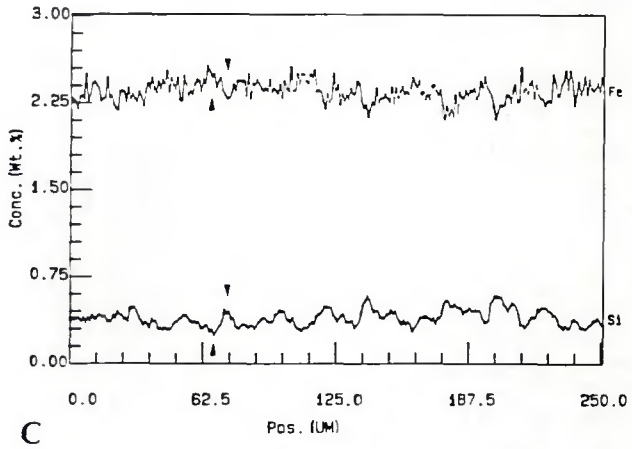

susceptibility of binary alloy systems from their equilibrium phase diagrams. Alloys that had extensive temperature separation between their liquidus and solidus were likely to be hot-crack sensitive. Using available binary phase diagrams, Borland developed a quantitative descriptor of the effect of a given alloying element on the equilibrium melting/solidification temperature range. He called this parameter the relative potency factor (Ref. 24) (RPF). It is defined as follows:

$$RPF = m_L(1-k)/k \quad (1)$$

where m_L is the liquidus slope and k is the equilibrium distribution coefficient. The units of the RPF are °C/wt-%. When the RPF is multiplied by the nominal alloy concentration, the equilibrium melting/solidification temperature range, ΔT_{eq}, results.

Table 5—Equilibrium Melting Temperature Range

Alloy No.	ΔT_{eq}
1	26.5 (0.6)[a]
2 (C)	33.7 (1.5)
3 (Si)	29.0 (1.6)
4 (C, Si)	43.3 (1.3)
5 (Nb)	55.3 (2.4)
6 (Nb, C)	72.8 (3.2)
7 (Nb, Si)	68.3 (2.5)
8 (Nb, C, Si)	76.3 (0.6)

(a) Values are averages of multiple tests; values in parentheses are standard deviations; all values in °C.

For the present alloys, the equilibrium melting temperature ranges, ΔT_{eq}, have been determined previously by Cieslak, *et al.* (Ref. 16). These data are listed in Table 5 and reveal that the Nb-bearing alloys (5–8) have a larger melting temperature range than the Nb-free alloys (1–4). (A melting temperature range for commercial Alloy 625 has been reported as ≈ 60°C/108°F—Ref. 25.) In particular, Alloy 1, the base alloy of the experiment, has an average ΔT_{eq} of only 26.5°C (48°F), in comparison to Alloy 5 (which contains the high level of Nb), which has a ΔT_{eq} of 55.3°C (100°F). A functional relationship between ΔT_{eq} and alloy composition was obtained (Ref. 16) by performing regression analysis on the data in Table 5, and is given below.

$$\Delta T_{eq}(°C) = 20.9 + 405.5\,(wt\text{-}\%\ C) + 20.3\,(wt\text{-}\%\ Si) + 9.4\,(wt\text{-}\%\ Nb) \quad (2)$$

The coefficient of correlation (R^2) for this relationship is 0.98 and the standard error is 3.0°C (5.4°F).

From these observations and perspectives, then, the hot-cracking response of the eight alloys examined here can begin to be understood. It is clear from examining Fig. 6 that the Nb-bearing alloys (5–8) are more susceptible to fusion zone hot cracking than are the Nb-free alloys (1–4). It is also clear that the least crack-sensitive alloy is Alloy 1, which has the lowest concentration of C, Si and Nb of any of the alloys examined. The results of regression analysis, given below, performed on the data shown in Fig. 6 reveal in more detail the functional relationship between the variable alloying elements (C, Si, Nb) and the MCL obtained during Varestraint testing.

$$MCL\,(in.) = 0.001 + 0.347\,(wt\text{-}\%\ C) + 0.037\,(wt\text{-}\%\ Si) + 0.007\,(wt\text{-}\%\ Nb) \quad (3)$$

The coefficient of correlation (R^2) for this relationship is 0.89 and the standard error is 0.006 in. (0.15 mm). A more complete description of the cracking behavior results when the interactive terms are included in the regression equation, as given below.

$$MCL\,(in.) = 0.008 + 0.235\,(wt\text{-}\%\ C) + 0.013\,(wt\text{-}\%\ Si) + 0.004\,(wt\text{-}\%\ Nb) + 0.068\,(wt\text{-}\%\ Nb)(wt\text{-}\%\ C) + 0.011\,(wt\text{-}\%\ Nb)(wt\text{-}\%\ Si) \quad (4)$$

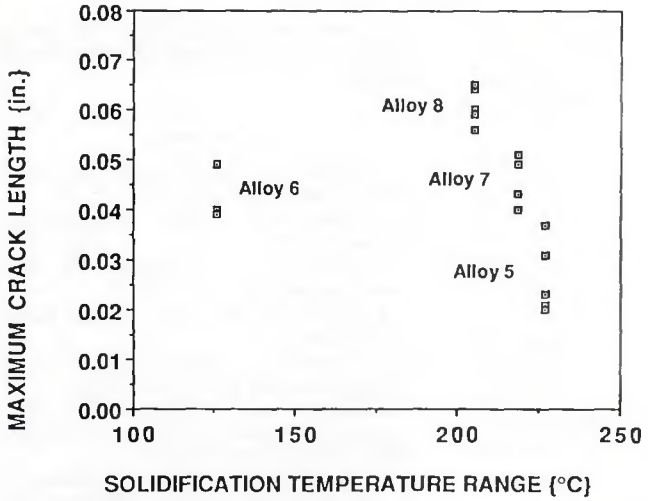

Fig. 10—Maximum crack length as a function of solidification temperature range for Alloys 5–8.

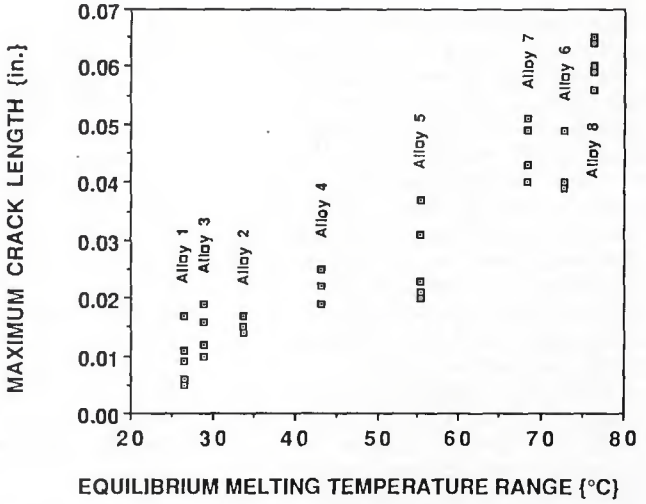

Fig. 11—Maximum crack length as a function of the equilibrium melting temperature range for Alloys 1–8.

The coefficient of correlation (R^2) for this relationship is 0.95 and the standard error is 0.004 in. (0.10 mm), a reduction of 50% from the standard error in Equation 3. Several implications may be drawn from Equations 3 and 4. The first is that additions of C, Si or Nb will increase the MCL, resulting in increased susceptibility to hot cracking. The second is that there are interactive effects between Nb and C and Nb and Si, both of which have the effect of increasing susceptibility to hot cracking. Finally, the largest effects are due solely to the presence of the individual alloying elements with interactive effects playing a lesser role. Although regression analysis does not explicitly create metallurgical interpretation, it does provide insight into potential chemical interactions, which manifest themselves as process-affecting metallurgical reactions. In the present case, interactions involving Nb and C (*i.e.*, γ/MC [NbC]) and Nb and Si (*i.e.*, γ/Laves and γ/M_6C) are suggested.

The TEM investigation revealed that all Nb-bearing alloys contained minor constituents, which could be referenced to the DTA thermograms shown in Figs. 1–4. Alloys 5, 7 and 8 contained Laves phase (Laves was the predominant microconstituent in Alloys 5 and 7) and all three had DTA indications at $\approx$ 1150°C. Alloys 6 and 8 contained MC (NbC) carbide as the predominant microconstituent and these two alloys had DTA indications at $\approx$ 1240°C (2264°F). Alloy 7 contained M_6C carbide having a lamellar morphology and a smaller indication on its DTA thermogram at 1206°C (2203°F).

With the DTA thermograms described as such, a direct classical interpretation of the weldability behavior based upon solidification temperature range might not seem unreasonable. Unfortunately, the data are not cooperative. Figure 10 shows the relationship between the solidification temperature range (ΔT_S) and MCL data for the Nb-bearing materials, Alloys 5–8. ΔT_S is defined as the temperature difference between the liquidus (taken from the on-heating data) and the temperature at which lowest melting point eutectic-type constituent forms. Even without performing a statistical analysis of these data, it is clear by observation that there is no strong functional correlation between these two quantities. From the ΔT_S data alone, it might be predicted that Alloy 6 would have the least susceptibility to hot cracking among the Nb-bearing alloys, but the MCL data does not bear this out. The lack of correlation between MCL and ΔT_S data also suggests that other factors are influencing the cracking phenomena.

Solidification cracking theory, as consolidated by Borland (Ref. 24), recognizes that several phenomena contribute to the hot cracking susceptibility of an alloy. In addition to solidification temperature range, the distribution and amount of terminal solidification liquid is important. The distribution of these liquids is primarily determined by their surface tensions. Liquids that have low surface tensions will have a tendency to spread out thinly and wet interdendritic and solidification grain boundaries. Terminal solidification liquids having a relatively large surface tension will have a tendency to spherodize locally, promoting solid bridging between adjacent dendrites or grains. Propagation of hot cracks along these boundaries will require fracture of these solid bridges, and thus will be less likely to occur from an energetics perspective. Implicit in this statement is the suggestion that cracking may terminate at a temperature above the terminal solid → liquid reaction temperature, even when high levels of strain are applied, if the distribution of liquid is not appropriate for crack advancement.

For a given alloy and specific eutectic constituent, hot cracking susceptibility increases with the amount of eutectic (Ref. 24) present up to a point where the phenomenon of eutectic healing begins. Eutectic healing occurs when there is a large enough amount of eutectic constituent present to effectively backfill or heal incipient hot cracks as they form. Many braze and solder alloys implicitly use the phenomenon of eutectic healing and thus are virtually immune from the problem of hot cracking during solidification. The amount of constituent necessary to fully affect eutectic healing is alloy dependent, but Clyne and Davies (Ref. 26) suggest that at least 10 vol-% is required. This value is supported by the work of Arata and coworkers (Ref. 27). They examined the effect of C additions on the weldability of 310 stainless steel. An alloy containing 0.43 wt-% C was found to contain 7 vol-% of the γ/M_7C_3 eutectic constituent. Trans-Varestraint tests revealed extensive hot cracking. An alloy containing 0.53 wt-% C was found to contain 11.5 vol-% of the γ/M_7C_3 eutectic constituent and exhibited only limited hot cracking. Metallographic analysis confirmed that eutectic healing was occurring.

In the present case, the amount of eutectic-type constituents in the various alloys can be suggested, at least semiquantitatively, from the DTA thermograms. Alloy 5, which experienced the least amount of hot cracking among the Nb-bearing alloys, clearly solidified with the least amount of eutectic constituent, which helps to explain at least in part its superior weldability. Among Alloys 6–8, more eutectic-type solidification is evident from their DTA thermograms. A rough estimate of the amount of constituents present can be made by integrating the areas under the peaks on the DTA thermograms corresponding to the eutectic-type reactions and ratioing them with the areas under the

matrix solidification peaks. The implicit assumption is that the volumetric enthalpies of solidification of the various constituents are similar, allowing for a ratio of areas to be equivalent to a ratio of volume fractions. For Alloys 6–8, this ratio is ≈ 3–5%. For Alloy 1 it is less than 1%. All of these values are less than the critical value given by Clyne and Davies (Ref. 26), suggesting that the condition for full eutectic healing is not reached. Metallography confirms this conclusion in that the region of backfilling observed in the Varestraint specimens was extremely limited.

Although the solidification temperature range, ΔT_S did not correlate well in this instance with the MCL data, an interesting correlation was observed between the MCL data and the equilibrium melting temperature range, ΔT_{eq}, data given in Table 5. It must be remembered that ΔT_{eq} is a phase diagram quantity. A plot of MCL as a function of ΔT_{eq} for the eight alloys examined is presented in Fig. 11. A reasonable functional relationship between these two quantities can be obtained, as given below the ΔT_{eq} in °C.

$$\text{MCL (in.)} = 8.7 \times 10^{-4} (\Delta T_{eq}) - 0.015 \quad (5)$$

The coefficient of correlation, R^2, for this expression is 0.86. This result confirms that to a large extent, the cracking behavior of this set of alloys under these experimental conditions is largely in response to the presence of the primary alloying variables, C, Si and Nb (see also Equations 2, 3). In particular, the presence of Nb at this concentration level is primarily responsible for the increase in ΔT_{eq} and thereby fundamentally diminishes the hot cracking resistance of these alloys in a manner consistent with that proposed by Borland (Ref. 24).

While the conclusions of this investigation can be generally applied, it must be remembered that the alloys used in this investigation were produced within a certain region of composition space in order to make the experimental matrix tractable. Extrapolation of the regression relations outside of the database for *quantitative* prediction is not recommended. Clearly, the presence of other alloying elements, such as boron, could have a large negative impact on the weldability of commercial alloys, while additions of Mn (as in Alloys 82 and 182) may help to improve weldability. For example, it has recently been suggested (Refs. 28, 29) that the role of boron in promoting hot cracking in nickel-based alloys is by acting as a surfactant for eutectic liquid films. From a slightly different perspective, the manner in which C, Si and Nb affect hot cracking may also involve influences on more subtle materials properties besides melting temperature range, such as solid/solid and solid/liquid surface tensions, properties which determine the distribution of liquids in the solidifying welds. It is clear that a better understanding of how chemistry influences these materials properties is necessary. Without these understandings, a completely self-consistent interpretation of collected hot cracking and solidification data is not possible, as was manifested by the inability to correlate MCL with ΔT_S data in a satisfactory manner in this work. From an engineering perspective, though, it is clear that the addition of reactive alloying elements (Nb, C, Si), which cause an increase in the melting/solidification temperature range and the formation of lower melting temperature eutectic-type constituents, leads to alloys having *fundamentally* diminished hot cracking resistance.

Conclusions

Among the alloys examined in this study, those containing intentionally alloyed Nb had terminal eutectic-type constituents involving MC (NbC) carbide, Laves phase and M_6C carbide. These alloys had a wider melting/solidification temperature range and diminished hot cracking resistance compared to alloys having essentially the same composition but not containing Nb. Among the Nb-bearing alloys, additions of C and Si were observed to both increase the amount of eutectic-type constituent present and to increase the susceptibility to hot cracking. Among the Nb-free alloys, C and Si additions increased both the melting/solidification temperature range and the susceptibility to hot cracking. A correlation was established between hot cracking susceptibility (MCL) and melting temperature range, ΔT_{eq}. From this correlation, it may also be inferred that within the composition range of Alloy 625, low-Nb-content heats will be less susceptible to hot cracking than high-Nb-content heats. Carbon alloying additions to the Nb-bearing alloys promoted the formation of the γ/MC (NbC) constituent at the expense of the γ/Laves constituent. Silicon promoted increased formation of the γ/Laves constituent with or without the presence of C and promoted the formation of a γ/M_6C constituent at low carbon levels.

Acknowledgments

The author wishes to acknowledge the following individuals for their assistance during the course of this investigation: T. J. Headley, G. A. Knorovsky, A. D. Romig, Jr., F. J. Zanner, T. J. Lienert, R. E. Semarge, M. E. McAllaster, W. R. Sorenson and T. Kollie. Special thanks is offered to C. V. Robino for helpful discussions and review of the study. This work was performed at Sandia National Laboratories, supported by the U.S. Dept. of Energy under contract number DE-AC04-76DP-00789.

References

1. Barker, J. F., Cox, J. D., and Margolin, E. 1968. *Metal Progress.* pp. 91–94.
2. Dimbylow, C. S. 1985. *Metal Construction.* pp. 35–39.
3. Bemst, A. V., and Dargent, Ph. 1983. *Metal Construction.* pp. 730–733.
4. Nugent, R. M. 1986. *Welding Journal* 65(6):33–39.
5. Patterson, R. A., and Milewski, J. O. 1985. *Welding Journal* 64(8):227-s to 731-s.
6. Robitz, E. S., Jr., and Edmonds, D. P. 1987. *Abstracts of Papers, 67th American Welding Society Meeting.* pp. 136–138.
7. Cieslak, M. J., Hills, C. R., and Headley, T. J. 1986. *Microbeam Analysis 1986.* San Francisco Press, Inc., pp. 69–72.
8. Lingenfelter, A. C. 1972. *Welding Journal* 51(9):430-s–436-s.
9. Arata, Y., Terai, K., Nagai, H., Shimizu, S., and Aota, T. 1977. *Trans. of JWRI.* 6(1):69–79.
10. Cieslak, M. J., Knorovsky, G. A., Headley, T. J., and Romig, A. D. Jr. 1986. *Metallurgical Transactions A.* pp. 2107–2116.
11. Wlodek, S. T. 1963. *Trans. Am. Soc. Met.*, Vol. 56, pp. 287–303.
12. Bastin, G. F., van Loo, F. J. J., and Heijligers, H. J. M. 1984. *X-ray Spec.* Vol. 31, p. 91.
13. Cliff, G. and Lorimer G. W. 1972. *Proc. 5th European Conf. on E. M.* Inst. of Physics, London, England, p. 140.
14. Romig, A. D., Jr. 1983. *Sandia National Laboratories Report SAND82-2983.*
15. Goldstein, J. I., Costley, J. L., Lorimer, G. W., and Reed, S. J. B. *SEN/1977* pp. 315–324.
16. Cieslak, M. J., Headley, T. J., Kollie, T., and Romig, A. D. Jr. 1988. *Metallurgical Transactions A.* Vol 19A, pp. 2319–2331.
17. Cieslak, M. J., and Savage, W. F. 1985. *Welding Journal* 64(5):119-s to 126-s.
18. Gehlbach, R. E., and Cook, S. W. 1970. Molten-salt reactor program semiannual report for period ending February 28, 1970. *ORNL Report No. 4548.*
19. Bardos, D. I., Gupta, K. P., and Beck, P. A. 1961. *Trans. TMS-AIME.* Vol. 221, p. 1087.
20. Nakao, Y., Oshige, H., Koga, S., Nishihara, H., and Sugitani, J. 1982. *Journal of the Japan Welding Society.* Vol. 51, No. 12, pp. 989–995.
21. Savage, W. F., and Lundin, C. D. 1966. *Welding Journal* 45(11):497-s to 503-s.
22. Matsuda, F., Nakagawa, H., Katayama, S., and Arata Y. 1982. *Trans. Japan Weld. Soc.* pp. 9–26.
23. Pumphrey, W. I., and Jennings P. H. 1948. *Jour. Inst. Metals.* Vol. 75, pp. 235–256.
24. Borland, J. C. 1960. *British Welding Journal.* Vol. 7, No. 8, pp. 508–512.
25. *Metals Handbook.* 9th ed., ASM, Materials Park, Ohio. Vol. 3, p 142.
26. Clyne, T. W., and Davies, G. J. 1979. *TMA Proc. Int. Conf. Solidification—Sheffield.* pp.275–278.
27. Arata, Y. Matsuda, F., and Katayama, S. 1977. *Trans. of JWRI.* pp.105–116.
28. Kelly, T. 1986. *Advances in Welding Science and Technology.* S.A. David, et., ASM International, pp. 623–628.
29. Cieslak, M. J., Stephens, J. J., and Carr, M. J. 1988. *Metallurgical Transactions A.* Vol. 19A, pp. 657–667.